Table 1 Aβ-like-peptides recovered from conditioned media of bafilomycin treated βAPP wt expressing cells

	Sequence	M.W. observed	M.W. calculated
Aβ (I^{-6}-V^{40})	ISEVKMDAEFRHDSGYEVHHQKLVFFAEDVGSNKGAIIGLMVGGVV	5018	(5017.7)
Aβ (V^{-3}-V^{40})	VKMDAEFRHDSGYEVHHQKLVFFAEDVGSNKGAIIGLMVGGVV	4688	(4688.4)

M.W., molecular weight.

K44A dynamin expression also affects extracellular cleavage site of βAPP

Bafilomycin is known to inhibit endocytosis through the inhibition of acidification of the luminal side of the vesicles.[21] Changes in extracellular cleavage of βAPP by bafilomycin treatment could be caused by the inhibition of endocytosis. To test this hypothesis, we used the K44A mutant of dymanin 1 which is reported to function as a dominant negative in endocytosis, because dynamin 1 is one of the essential molecules for endocytosis.[19] Expression of dynamin K44A mutant inhibits endocytosis by about 70%.[19,22] We analyzed the conditioned media of dynamin K44A and βAPP sw expressing HeLa cells. As shown in the lower panels of Figure 2B, these cells also secreted significant amounts of Aβ (V^{-3}-V^{40}) and Aβ (I^{-6}-V^{40}). These results together suggested that the inhibition of endocytosis causes changes in the extracellular cleavage sites of both βAPP wt and sw in a similar manner, that is, decreasing the D^1 cleavage and increasing the V^{-3} and I^{-6} cleavages. In Figure 2C, the effect of suppression of endocytosis either by bafilomycin treatment or the dominant negative mutant of dynamin 1 is illustrated. In the physiological conditions, D^1 site cleavage is dominant and a small amount of V^{-3} and I^{-6} cleavages are observed. In the situation where endocytosis is inhibited, the V^{-3} and I^{-6} sites become more significant and D^1 site cleavage results in a minor peak with K293 cells expressing wt βAPP as well as βAPP sw (Fig. 2C).

Cleavage precision by γ-secretase is conserved even when the N-termini of CTF-stubs are elongated

CTF-stubs of βAPP are thought to be promptly cleaved by γ-secretase to generate heterogeneous C-termini of Aβ.[1] As shown in Figure 3A, several γ-cleavage sites (γ40, γ42) are known, and the increased ratio of γ42/γ40 is recognized as a pathological hallmark of AD. Change in the precision of γ-cleavage can be monitored by measuring the amount of secreted Aβ (D^1-A^{42}). It is interesting to test whether the γ-secretase precision change may be affected in the case of N-terminally elongated Aβ starting from V^{-3} and I^{-6}. For this purpose, we prepared PS1 L166P pathogenic mutant expressing cells, which affect γ-cleavage precision as a mutant effect.[18] As shown in Figure 3B and C, left panels, in PS1 L166P expressing cells, elevation of Aβ (D^1-A^{42}) was observed compared to that of wt PS expressing cells. It is to be noted that the peak height of Aβ (V^{-3}-A^{42}) and Aβ (I^{-6}-A^{42}) was also observed by bafilomycin treatment (Fig. 3B,C right panels). The bafilomycin-induced increase at V^{-3} and I^{-6} is observed with γ42 fragments caused by PS1 mutation. This result indicates that C-terminus of Aβ-like-peptides with N-terminus starting from V^{-3} and I^{-6} is also decided by γ-secretase with precision similar to that of Aβ starting from D^1.

α-Secretase stimulant PMA did not affect I^{-6} and V^{-3} cleavages, whereas β-secretase inhibitor showed different effects on V^{-3} and I^{-6} cleavage

Finally, we tried to investigate the characteristics of V^{-3} and I^{-6} cleavage. The majority of the βAPP extracellular domain cleavage site is classified into either α- or β-secretase. We investigated whether I^{-6} and V^{-3} cleavage is due to α- and/or β-secretase. First, PMA, α-secretase stimulant, was added to βAPP sw expressing cells. As shown in the left panel of Figure 4A, consistent with a previous report,[23] the peak height of P3 (L^{17}-V^{40}) was increased compared to that of untreated example (Fig. 4C left panel), indicating PMA treatment stimulates α-secretase activity. However, in the same media, peak heights of Aβ (V^{-3}-V^{40}) and Aβ (I^{-6}-V^{40}) did not increase (Fig. 4A right panels), indicating no effect of α-secretase activation. Next, we analyzed the effect of z-VLL-CHO, a β-secretase inhibitor. The peak height of Aβ (I^{-6}-V^{40}) was almost the same as that of the untreated sample (Fig. 4C right panel), while the peak height of Aβ (V^{-3}-V^{40}) is slightly decreased (Fig. 4B right panel). These results indicate I^{-6} cleavage of βAPP is not mediated by α- and β- secretase, while cleavage at V^{-3} position is associated with β-secretase.

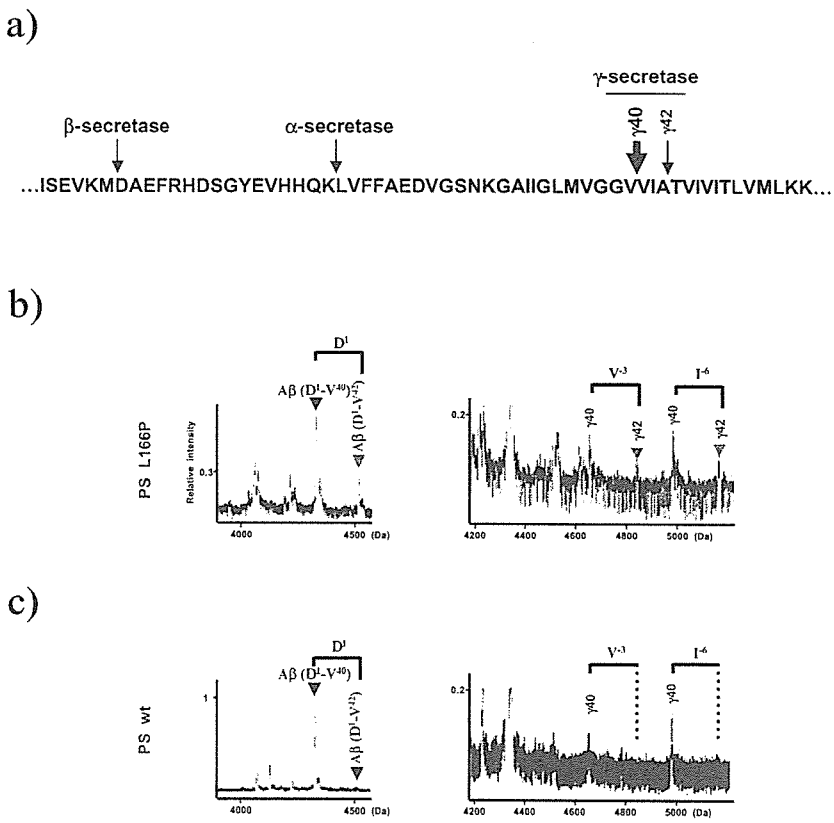

Figure 3 Effect of PS1 L166P expression on Aβ and N-terminally elongated Aβ secretion. (A) Schematic presentation of α/β/γ-secretase cleavage site of βAPP. Each cleavage site by α/β/γ-secretase is shown. γ-cleavage has diversity mainly at γ40 and γ42. The gray box denotes the transmembrane domain of βAPP. Mass spectra of Aβ from bafilomycin treated PS1 L166P (B) or wt (C) and βAPP sw expressing cells. Red arrows indicate elevated peaks compared with that of PS1 wt expressing cells. Molecular masses of each peak are shown in.

Table 2 Aβ-like-peptides recovered from conditioned media of bafilomycin treated βAPP sw expressing cells

	Sequence	M.W. observed	M.W. calculated
Aβ (I^{-6}-V^{40})	ISEVNLDAEFRHDSGYEVHHQKLVFFAEDVGSNKGAIIGLMVGGVV	4985	(4985.6)
Aβ (I^{-6}-V^{40})	VNLDAEFRHDSGYEVHHQKLVFFAEDVGSNKGAIIGLMVGGVV	4656	(4656.3)

M.W., molecular weight.

Table 3 Aβ-like-peptides recovered from conditioned media of bafilomycin treated βAPP sw and PS1 L166P expressing cells

	Sequence	M.W. observed	M.W. calculated
Aβ (D^{1}-A^{42})	DAEFRHDSGYEVHHQKLVFFAEDVGSNKGAIIGLMVGGVVIA	4514	(4514.1)
Aβ (V^{-3}-A^{42})	VNLDAEFRHDSGYEVHHQKLVFFAEDVGSNKGAIIGLMVGGVVIA	4840	(4840.5)
Aβ (I^{-6}-A^{42})	ISEVNLDAEFRHDSGYEVHHQKLVFFAEDVGSNKGAIIGLMVGGVVIA	5170	(5169.8)

M.W., molecular weight.

DISCUSSION

We investigated the mode of extracellular shedding of βAPP at V^{-3} and I^{-6} in details. Our data indicate that endocytosis inhibition may up-regulate cleavages at V^{-3} and I^{-6}, since both bafilomycin treatment and the expression of dominant negative dynamin mutant increase V^{-3} and I^{-6} cleavages. A relatively weak increase of V^{-3} and I^{-6} cleavages by K44A dynamin expression compared with bafilomycin treatment might be due to a reduced inhibition level of endocytosis, since ~70% of endocytosis in the cells is inhibited upon expression of the dynamin K44A mutant.[19,22] It can be considered that suppression of endocytosis may be associated with the level of V^{-3} and I^{-6} cleav-

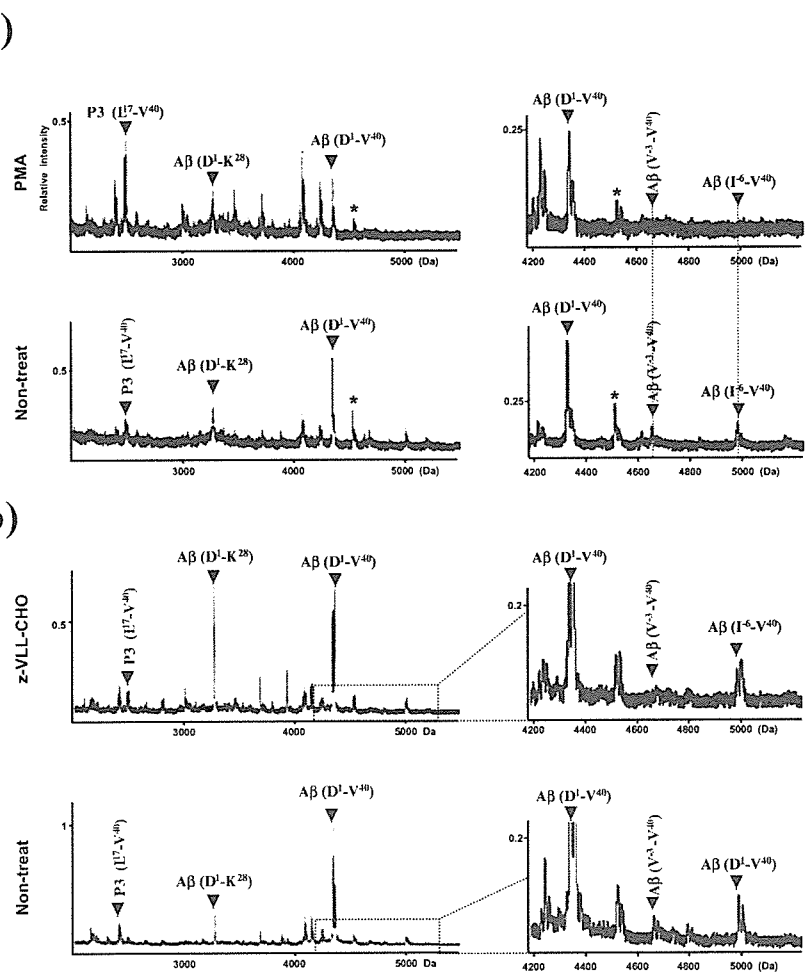

Figure 4 Effect of PMA and z-VLL-CHO on Aβ-like-peptides secretion. Mass spectra of Aβ-like-peptides immunoprecipitated from conditioned media of bafilomycin treated βAPP sw expressing cells additionally treated with or without PMA (A) or z-VLL-CHO (B). Each right panel shows high magnification of left panel of indicated mass range. (A) βAPP sw and PS1 L166P expressing K293 cell were used. (B) βAPP sw expressing K293 cell were used. Molecular masses of each peak are shown in Table 3.

ages. Since suppression of endocytosis results in processing of βAPP more on the plasma membrane, V^{-3} and I^{-6} may be cleaved on the plasma membrane.

α-Cleavage at L^{17} of βAPP is known to occur on the plasma membrane. Therefore, we considered the possibilities that V^{-3} and I^{-6} cleavage may be mediated by α-secretase. PMA treatment, however, which up-regulates expression and activity of α-secretase, increased neither V^{-3} nor I^{-6} cleavages, indicating that these cleavages were mediated by secretases other than α-secretase. We then tried to determine whether these cleavages were mediated by β-secretase. Interestingly, β-secretase inhibitor treatment caused different effects on V^{-3} and I^{-6} cleavages. The I^{-6} cleavage was not affected, while the V^{-3} cleavage was suppressed by inhibitor treatment. Therefore, the V^{-3} cleavage of βAPP may be considered to be associated with β-secretase. However, it is of note that the I^{-6} cleavage might be mediated by neither α- nor β-secretase, suggesting the involvement of a novel unidentified secretase in the process of βAPP cleavage. Since the resultant βAPP-CTF stubs by this extracellular shedding undergoes subsequent intramembrane proteolysis by γ-secretase, our data demonstrates a novel alternative degradation process of βAPP without α- and β-secretase activities.

Precision of γ-cleavage is important in the pathogenesis of AD because up-regulation of Aβ42 (Aβ (D^1-A^{42})) is consistently observed in AD as well as model animals. In this study, we have demonstrated that suppression of endocytosis results in an increased amount of V^{-3} and I^{-6} fragments in wt βAPP expressing cells as well as in cells with FAD linked mutations, βAPP sw, PS1 L166P. The increases in V^{-3} and I^{-6} cleavages are observed with γ42 fragments caused by PS1 L166P mutation. Therefore, the different

cleavage at N-terminal of Aβ is not closely related with pathogenic mutations of AD. It is to be noted that the Swedish mutation that is a substitute for K^{-2} and M^{-1} to N^{-2} and L^{-1} between D^{1} and V^{-3} does not affect the cleavage of the N-terminal of Aβ. Therefore, we suggest that extracellular shedding of βAPP at V^{-3} and I^{-6}, occurring on the plasma membrane, does not seem to affect the precision of γ-secretase cleavage.

We propose that the process of N-terminally elongated Aβ species generation is not directly linked to the phenotype due to AD associated PS and βAPP mutants.

REFERENCES

1 Selkoe DJ. Alzheimer's disease: genes, proteins, and therapy. *Physiol Rev* 2001; **81**: 741–766.
2 Lammich S, Kojro E, Postina R *et al.* Constitutive and regulated alpha-secretase cleavage of Alzheimer's amyloid precursor protein by a disintegrin metalloprotease. *Proc Natl Acad Sci USA* 1999; **96**: 3922–3927.
3 Koike H, Tomioka S, Sorimachi H *et al.* Membrane-anchored metalloprotease MDC9 has an alpha-secretase activity responsible for processing the amyloid precursor protein. *Biochem J* 1999; **343** (Pt 2): 371–375.
4 Buxbaum JD, Liu KN, Luo Y *et al.* Evidence that tumor necrosis factor alpha converting enzyme is involved in regulated alpha-secretase cleavage of the Alzheimer amyloid protein precursor. *J Biol Chem* 1998; **273**: 27765–27767.
5 Sisodia SS. Beta-amyloid precursor protein cleavage by a membrane-bound protease. *Proc Natl Acad Sci USA* 1992; **89**: 6075–6079.
6 Haass C, Schlossmacher MG, Hung AY *et al.* Amyloid beta-peptide is produced by cultured cells during normal metabolism. *Nature* 1992; **359**: 322–325.
7 Vassar R, Bennett BD, Babu-Khan S *et al.* Beta-secretase cleavage of Alzheimer's amyloid precursor protein by the transmembrane aspartic protease BACE. *Science* 1999; **286**: 735–741.
8 Sinha S, Anderson JP, Barbour R *et al.* Purification and cloning of amyloid precursor protein beta-secretase from human brain. *Nature* 1999; **402**: 537–540.
9 Yan R, Bienkowski MJ, Shuck ME *et al.* Membrane-anchored aspartyl protease with Alzheimer's disease beta-secretase activity. *Nature* 1999; **402**: 533–537.
10 Hussain I, Powell D, Howlett DR *et al.* Identification of a novel aspartic protease (Asp 2) as beta-secretase. *Mol Cell Neurosci* 1999; **14**: 419–427.
11 Lin X, Koelsch G, Wu S, Downs D, Dashti A, Tang J. Human aspartic protease memapsin 2 cleaves the beta-secretase site of beta-amyloid precursor protein. *Proc Natl Acad Sci USA* 2000; **97**: 1456–1460.
12 Takeda K, Araki W, Akiyama H, Tabira T. Amino-truncated amyloid beta-peptide (Abeta5-40/42) produced from caspase-cleaved amyloid precursor protein is deposited in Alzheimer's disease brain. *FASEB J* 2004; **18**: 1755–1757.
13 Liu K, Doms RW, Lee VM. Glu11 site cleavage and N-terminally truncated A beta production upon BACE overexpression. *Biochemistry* 2002; **41**: 3128–3136.
14 Yan R, Munzner JB, Shuck ME, Bienkowski MJ. BACE2 functions as an alternative alpha-secretase in cells. *J Biol Chem* 2001; **276**: 34019–34027.
15 Haass C, Capell A, Citron M, Teplow DB, Selkoe DJ. The vacuolar H(+)-ATPase inhibitor bafilomycin A1 differentially affects proteolytic processing of mutant and wild-type beta-amyloid precursor protein. *J Biol Chem* 1995; **270**: 6186–6192.
16 Steiner H, Romig H, Pesold B *et al.* Amyloidogenic function of the Alzheimer's disease-associated presenilin 1 in the absence of endoproteolysis. *Biochemistry* 1999; **38**: 14600–14605.
17 Okochi M, Eimer S, Bottcher A *et al.* A loss of function mutant of the presenilin homologue SEL-12 undergoes aberrant endoproteolysis in Caenorhabditis elegans and increases abeta 42 generation in human cells. *J Biol Chem* 2000; **275**: 40925–40932.
18 Moehlmann T, Winkler E, Xia X *et al.* Presenilin-1 mutations of leucine 166 equally affect the generation of the Notch and APP intracellular domains independent of their effect on Abeta 42 production. *Proc Natl Acad Sci USA* 2002; **99**: 8025–8030.
19 Damke H, Baba T, Warnock DE, Schmid SL. Induction of mutant dynamin specifically blocks endocytic coated vesicle formation. *J Cell Biol* 1994; **127**: 915–934.
20 Okochi M, Steiner H, Fukumori A *et al.* Presenilins mediate a dual intramembranous gamma-secretase cleavage of Notch-1. *EMBO J* 2002; **21**: 5408–5416.
21 Stevens TH, Forgac M. Structure, function and regulation of the vacuolar (H+)-ATPase. *Annu Rev Cell Dev Biol* 1997; **13**: 779–808.
22 Chyung JH, Selkoe DJ. Inhibition of receptor-mediated endocytosis demonstrates generation of amyloid beta-protein at the cell surface. *J Biol Chem* 2003; **278**: 51035–51043.
23 Hung AY, Haass C, Nitsch RM *et al.* Activation of protein kinase C inhibits cellular production of the amyloid beta-protein. *J Biol Chem* 1993; **268**: 22959–22962.

ORIGINAL ARTICLE

Aβ induces endoplasmic reticulum stress causing possible proteasome impairment via the endoplasmic reticulum–associated degradation pathway

Daisuke KANAYAMA,[1] Takashi KUDO,[1] Ryo KIMURA,[1] Nobuhiko TABUCHI,[1] Akio FUKUMORI,[1] Takeshi MORIHARA,[1] Shinji TAGAMI,[1] Hisashi TANII,[4] Masayasu OKOCHI,[1] Kojin KAMINO,[1] Toshihisa TANAKA,[1] Kazunori IMAIZUMI,[2] Takeshi TABIRA[3] and Masatoshi TAKEDA[1]

[1]Department of Post-Genomics and Diseases, Division of Psychiatry and Behavioral Proteomics, Osaka University Graduate School of Medicine, Osaka, [2]Division of Molecular and Cellular Biology, Department of Anatomy, Faculty of Medicine, University of Miyazaki, Miyazaki, and [3]National Institute for Longevity Sciences, National Center for Geriatrics and Gerontology, Obu, [4]Department of Psychiatry, Mie University Graduate School of Medicine, Tsu, Japan

Correspondence: Takashi Kudo PhD, Department of Post-Genomics and Diseases, Division of Psychiatry and Behavioral Proteomics, Osaka University Graduate School of Medicine, D3, 2-2 Yamadaoka, Suita, Osaka 565-0871, Japan. Email: kudo@psy.med.osaka-u.ac.jp

Received 28 December 2005; accepted 16 January 2006.

Key words: *Alzheimer's disease, amyloid-β, proteasome, unfolded protein response.*

Abstract

Background: Accumulation of β-amyloid is a major pathology of Alzheimer's disease (AD). As in other neurodegenerative diseases, it is also reported that proteasome activity is deteriorated in post-mortem brains of AD patients. However, the mechanism of proteasomal dysfunction in AD remains unexplained. There is, however, increasing reported evidence that the unfolded protein response (UPR) is involved in AD pathology. Here we show that Aβ causes not only the UPR leading to endoplasmic reticulum (ER) stress mediated cell death, but also proteasomal dysfunction in cultured cells.

Methods: Mouse primary cultured neurons and other cultured cells such as HEK 293T or SH-SY5Y were treated with Aβ or other reagents, such as thapsigargin and lactacystin, to study UPR or proteasome activity. The UPR was investigated using proteins or mRNA expression. To ascertain proteasome activity, we also recruited SH-SY5Y cells stably transfected with GFP^u.

Results: *In vitro* study showed that UPR, phosphorylation of eIF-2α and BiP degradation preceded proteasome dysfunction. It is known that the UPR of ER occurs with the assistance of proteasome as ER-associated protein degradation (ERAD).

Conclusion: This evidence, taken together, suggests that Aβ may induce proteasome dysfunction by preceding the UPR through ER-associated protein degradation.

INTRODUCTION

Although Alzheimer's disease (AD) is characterized by progressive neurodegeneration in the brain, the causes and mechanisms of neuronal loss have yet to be elucidated. Two types of abnormal protein deposits are observed pathologically in AD-patient brains; neurofibrillary tangles (NFT) and extracellular amyloid plaques, with their main components being tau-forming paired helical filament (PHF) and amyloid β peptide (Aβ), respectively. Aβ is produced from amyloid precursor protein (APP) by sequential proteolysis of β- and γ-secretase.[1] Presenilin-1 (PS1) complex has recently been shown to be responsible for this γ-secretase activity.[2,3]

In familial Alzheimer's disease (FAD), linked mutations of PS1, the altered proteolytic processing of APP causes the elevation of Aβ; Katayama *et al.* reported that PS1 mutants may down-regulate the unfolded protein response (UPR), the mechanism that responds to the accumulation of unfolded proteins in the endoplasmic reticulum (ER) by ER stress, to increase cell vulnerability.[4]

The UPR is known as the mechanism managing quality control of protein production and maturation in the ER.[5,6] Cells are sometimes attacked by various stresses such as starvation, ischemia and oxidative stress. Under such conditions, protein synthesis and maturation in the ER is confused so that unusually misfolded proteins emerge and accumulate in the ER. The UPR is a mechanism that eliminates these misfolded proteins by re-folding them with chaperone proteins such as BiP/GRP78, or by attenuating protein synthesis with PERK phosphorylated eIF-2α. On the other hand, ER stress also activates apoptosis by JNK phosphorylation and ER resident caspase-4/12 activation.[7–9]

There is also a proposed mechanism called ER-associated protein degradation (ERAD), a proteasome-mediated protein degradation mechanism, which degrades the unfolded proteins in the proteasome to help clear them in the ER.[6,10,11] Several proteins are reported as essential for ERAD; for instance, BiP, protein disulfide isomerase family proteins and the Sec61p translocon are necessary for carrying these misfolded proteins out of the ER.[12] After their translocation to the cytosol, they are polyubiquitinated to promote accumulation in the proteasome and are then degraded. Thus degradation in the proteasome is now considered to be an important component in the UPR.

Proteasomes play a key role in many neurodegenerative diseases, such as Parkinson and polyglutamine diseases.[13,14] Some reports have shown that the ubiquitin–proteasome system (UPS) is the main target of the pathological events observed in the brain such as inclusion body or extracellular deposits.[13,14]

As with other neurodegenerative diseases, reports about the involvement of proteasomes in the pathology of AD have increased. Keller *et al.* showed that proteasome activity in a region-of-interest (e.g., hippocampus and related limbic structures and the inferior parietal lobe) is reduced in post-mortem brain tissue in AD patients.[15] These reports suggest that a disturbance of proteasome function may be provoked in AD brains, and as a result may accelerate the pathological process.

Here we investigated Aβ toxicity of these two adjacent mechanisms – the UPR and proteasome activity – to determine which is more dominantly involved.

MATERIALS AND METHODS

Cell culture

To establish permanent cell lines, HEK293T or SH-SY5Y cells were stably transfected with human wild type APP or Swedish mutant APP, or GFP^u. For GFP^u, pEGFPu plasmid in E. coli was purchased from ATCC (Manassas, USA).

Primary culture

Primary cultured neurons were obtained from 12.5-day mouse embryos. Dissociated cells were allowed to mature for 5 days in neurobasal medium (Gibco, Invitrogen, Carlsbad, CA, USA), then cultured cells were used for the experiments.

Aβ preparation and treatment

Thapsigargin, MG132 and lactacystin were purchased from Sigma Aldrich (St. Louis, MO), and epoxomicin from Calbiochem (Dermstadt, Germany). These reagents were prepared in 1 mM DMSO and diluted in culture media to indicated concentrations. Aβ25-35 and Aβ1-40 were also purchased from Sigma and incubated at 37°C for 72 h to facilitate its aggregation before being added to cell culture media. Cells were pre-incubated with fresh media for 1 h and treated with the aggregated Aβ or the indicated reagents containing media.

Antibodies

Antiphospho eIF-2α antibody was purchased from Cell Signaling (Beverly, MA, USA), antiphospho JNK from Promega (Madison, WI, USA), anticaspase-12 from Exalpha Biologicals (Maynard, MA, USA), anti-PERK from Qiagen (Valencia, CA, USA) and anti-GFP from MBL (Medical & Biological Laboratories, Nagoya, Japan). Every antibody was used at the concentrations indicated in the manufacturer's instructions.

Lysis and Western blotting

Cells were harvested and lyzed by the lysis buffer (20 mM HEPES, pH 7.5, 150 mM NaCl, 1% triton-X100, 10% glycerol, 1 mM EDTA 10 mM tetrasodium pyrophosphate, 100 mM NaF, 17.5 mM beta-glycerophosphate, 1 mM phenylmethysulfonyl fluoride, 4 mg/mL aprotonin and 2 mg/mL pepstatin A). Then lysates were centrifuged at 14 000 rpm for 15 min at 4°C. Protein concentration of the supernatants was determined and an equal amount of each sample was applied for SDS-PAGE followed by immunoblotting.

Lactate dehydrogenase assay

Lactate dehydrogenase (LDH) levels in culture medium were quantified as described.[16]

Northern blotting

RNA was isolated from cultured cells with RNeasy kit (Qiagen) after indicated stimulation with Aβ. Each of the isolated RNA were applied to electrophoresis and then transferred to nitrocellulose membrane, immobilin-Ny+ (Millipore, Bedford, MA, USA). An RNA probe for GRP78 mRNA was prepared from GRP78-pBluescript with random primer kit (Takara, Tokyo, Japan) and 32P-dCTP (Amersham, Piscataway, NJ, USA).

Proteasome activity

Approximately 5×10^6 cells were lyzed in the lysis buffer (50 nM Tris-HCl (pH 7.5), 100 mM NaCl, 0.2% CHAPS, 5 mM EDTA, 1 mM EGTA, 3 mM NaN3, and protease inhibitor cocktail (Sigma)) after the indicated stimulation, and cell extracts were clarified by centrifugation at 45 000 rpm for 30 min at 4°C. The chymotrypsin-like peptidase activity of the proteasome was measured using the Succinil-Leu-Leu-Val-Tyr-7 amino-4-methylcoumarin (Suc-LLVY-MCA, Bachem, Bubendorf, Switzerland) as a substrate. Eighty milliliters of cell extract and 100 μL of 50 nM Suc-LLVY-AMC were mixed and incubated for 15 min at 37°C. Fluorescence of the released amino-4-methylcoumarin (AMC) was measured at an excitation wavelength of 380 nm and an emission wavelength of 450 nm.

RESULTS

Aβ causes endoplasmic reticulum stress and endoplasmic reticulum stress mediated cell death

Aβ25-35/35-25 or Aβ1-40/40-1 peptides were added to a culture media of SK-N-SH cells to see whether Aβ induces ER stress. Western blotting showed that Aβ25-35 or Aβ1-40 treatment phosphorylates eIF-2α, but the reverse peptides do not (Fig. 1a). PERK is also phosphorylated by Aβ25-35, but not by Aβ35-25 (Fig. 1b). Northern blot showed that the transcription of GRP78 was induced by Aβ 25-35 but not by the reverse peptides (Fig. 1c). These data show that added Aβ causes ER stress.

To determine whether this ER stress by Aβ caused neuronal cell death, mouse primary neurons are treated with Aβ and apoptotic signal transduction was investigated. The cleavage of caspase-12 was observed only when cells were treated with Aβ25-35 (Fig. 1d). To confirm that cell death is actually induced by Aβ, LDH assay was performed and it was found that Aβ25-35 and Aβ1-40 increase LDH release (Fig. 1e). These data indicate that extracellular Aβ25-35 may cause neuronal cell death through apoptosis mediated by ER stress.

Endoplasmic reticulum stress and proteasomal dysfunction affect each other

We treated SH-SY5Y cells with Aβ1-40 or Aβ1-42 at the indicated concentration (Fig. 2a). Proteasomal activity reduced both Aβ1-40 or Aβ1-42 to about 50% compared to controls. To confirm these effects of Aβ on proteasome, we used cells transiently transfected with GFP^u, which is immediately degraded by proteasome under normal conditions, but is accumulated when proteasome is disturbed.[17] Specific proteasome inhibitors such as epoxomicin and lactacystin induced the accumulation of GFP^u (Fig. 2b). Aβ1-40 also induced the accumulation of GFP^u in a dose-dependent manner suggesting that proteasomal dysfunction may be caused by Aβ (Fig. 2b). Interestingly, the ER stress inducer thapsigargin could to some extent also induce this accumulation (Fig. 2b).

Proteasome inhibition induces unfolded protein response

To obtain clues whether Aβ independently affects the UPR and proteasomal dysfunction or not, we studied whether inhibition of proteasomal activity may cause the UPR. BiP induction and cleavage of caspase-4 occurred in cells treated with proteasome inhibitors (Fig. 3a,b), suggesting that inhibition of proteasome may cause ER stress. In addition, ER stress induction by lactacystin was more prominent in cells expressing swAPP, suggesting that ER stress by proteasome dysfunction is accelerated by Aβ. This phenomenon was confirmed by a study of the dose-dependent effect of lactacystin on phosphorylation of eIF-2α (Fig. 3c,d). Again, both lactacystin and Aβ1-40 treatment more potently phosphorylated eIF-2α, indicating that with Aβ1-40 treatment inhibition of proteasome may cause ER stress.

Proteasome inhibition arises from and after the unfolded protein response

As demonstrated in Fig. 2, thapsigargin causes GFP^u accumulation, indicating that proteasome dysfunction

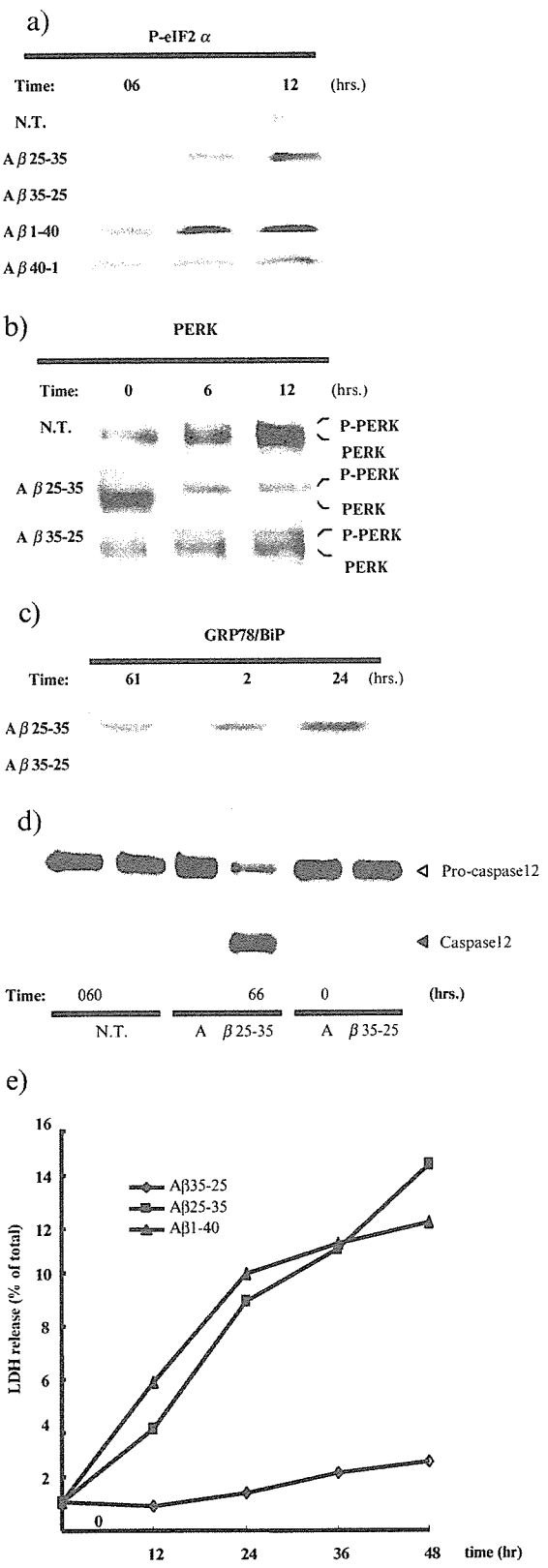

Figure 1 Aβ induces the UPR to activate ER-mediated cell death. (a) SK-N-SH cells were treated with 25 μM Aβ25-35, 10 μM Aβ1-40 or their reverse peptides. Western blotting shows that eIF-2a phosphorylation is observed when cells are treated with 25 μM Aβ25-35 or 10 μM Aβ1-40, but reverse peptide does not induce phosphorylation. (b) PERK is also phosphorylated with Aβ25-35, but not Aβ35-25. Phosphorylated PERK can be seen as shifted bands. (c) Northern blotting for GRP78 indicates that GRP78 gene transcription is induced by 25 μM Aβ25-35, whereas treatment with reverse peptide causes no induction. (d) Western blot of mouse primary cultured neuronal cells shows that cleavage of caspase-12 is observed only in cells treated with 25 μM Aβ25-35. (e) LDH assay indicates that 25 μM Aβ25-35 and 10 μM Aβ1-40 causes LDH release, while Aβ35-25 treatment induces almost no changes.

was induced by the UPR. Thus we investigated the relationship between the UPR and proteasome function in a time–course study (Fig. 4). We observed the phosphorylation of eIF-2α primarily occurred at 15 min, then the induction of BiP expression followed one hour after treatment. After the UPR had occurred

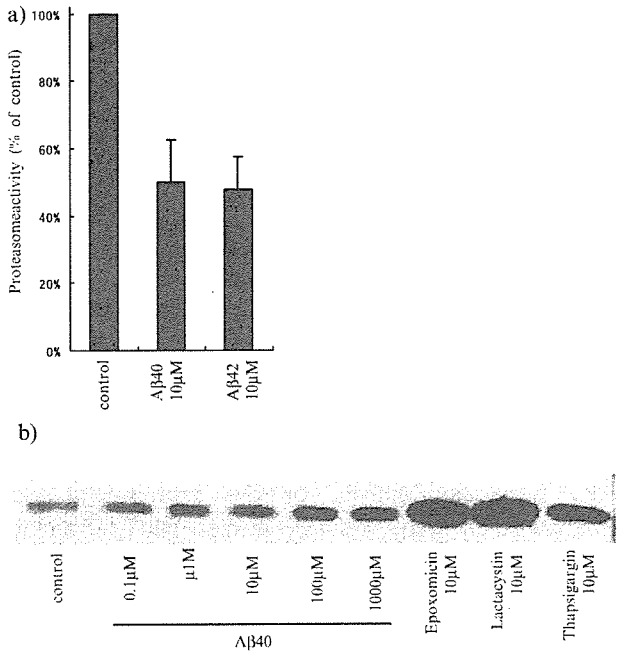

Figure 2 Proteasomes are disturbed by Aβ in a dose-dependent manner. SH-SY5Y(–) cells were treated with Aβ or indicated reagents at indicated doses for 24 h. Treatment with extracellular Aβ has a deleterious effect on proteasomal activity. (a) Aβ1-40 and Aβ1-42 can, respectively, reduce proteasomal activity to about 50% of control. Proteasome activity was measured using Luc-LLVY-AMC. (b) Western blot of transiently transfected GFP^u, which is accumulated under Aβ40, proteasome inhibitor, epoxomicin and lactacystin, and ER stress inducer thapsigargin. Note that Aβ40 causes GFP^u accumulation in a dose-dependent manner.

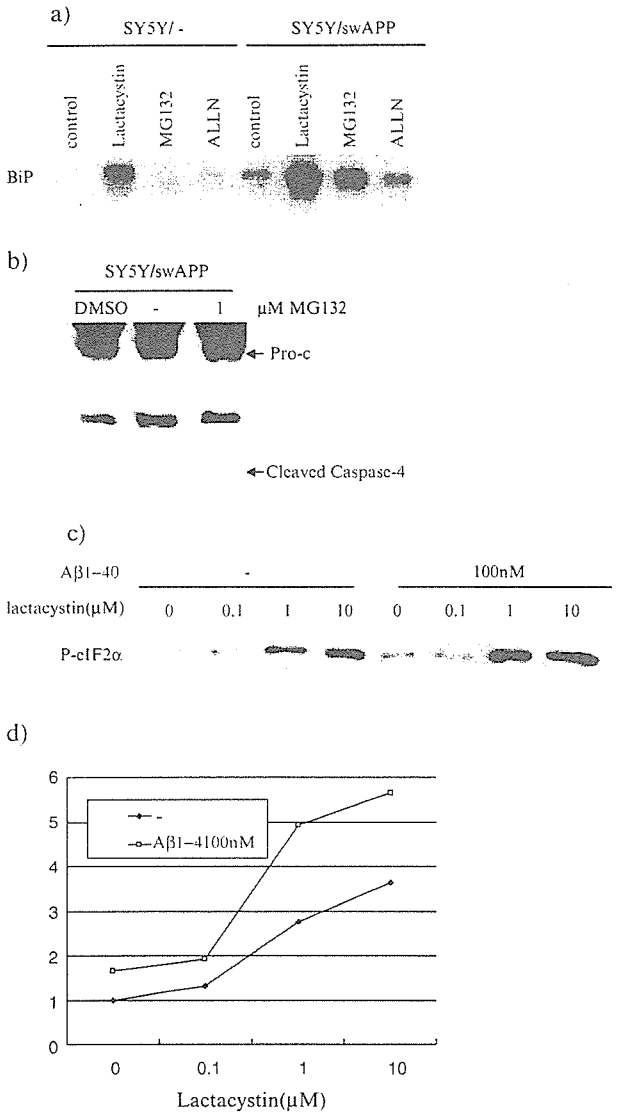

Figure 3 ER stress is caused by proteasomal dysfunction, which is modified by Aβ. Proteasome inhibition induces UPR and this response is accelerated by Aβ. (a) Northern blotting of BiP shows that proteasome inhibitors cause the UPR. SH-SY5Y(–) and SH-SY5Y(swAPP) cells treated with 10 μM lactacystin, 10 μM MG132 and 10 μM ALLN for 24 h. Transcription induction of BiP is induced by proteasome inhibitors. (b) Cleavage of caspase-4 is also induced by MG132 treatment for 24 h. (c) Dose dependent induction of the UPR by lactacystin and the synergistic effect of Aβ after 24 h of treatment is shown. Western blotting shows lactacystin causes eIF-2α phosphorylation, which is enhanced by Aβ treatment. (d) A densitometric scan of phosphorylated eIF-2α levels is shown in panel (c). Each band of the Western blot is digitized by densitometry.

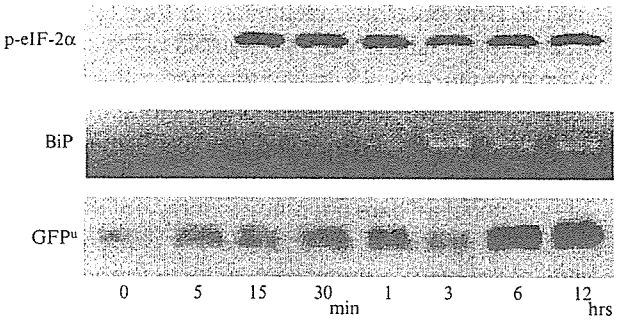

Figure 4 SH-SY5Y(GFP^u) cells were treated with 10 μM thapsigargin and followed over the indicated time. Phosphorylation of eIF-2α, BiP induction and GFP^u accumulation can be observed from 15 min, 1 h and 6 h, respectively.

thoroughly, GFP^u accumulation was observed after six hours. These data showed that the UPR may precede proteasome inhibition.

DISCUSSION

Katayama *et al.* showed that PS1 mutations in FAD alters the UPR and increases vulnerability to ER stress.[4] Nakagawa *et al.* reported that in rodents Aβ induces apoptosis via caspase-12, which is an ER-resident caspase and ER-specific apoptotic signaling cascade mediator.[7] We previously reported that caspase-4 is the human homolog of caspase-12 and that caspase-4 also transduces ER-mediated apoptotic signals.[9] These findings moved us to investigate the relationship between the Aβ burden and the UPR, which ultimately induces apoptosis.

Proteasome is strongly related to the UPR because there is a putative mechanism called ERAD, which refers to proteasomes as a bulk degradation system of the misfolded protein accumulated in ER. Our data shows that proteasomes are actually involved in the Aβ cytotoxicity associated with the UPR; this is the first evidence to explain the relationship between Aβ, the UPR and the alteration of proteasomal activity in AD brain.

Our data suggest that Aβ causes ER stress and proteasomal dysfunction, which means that extracellular Aβ alters these intracellular systems. It has been reported that Aβ1-42 internalization occurs via a phagocytic process and that Aβ1-42 accumulates in macrophages.[18] It has also been indicated that intracellular accumulation of Aβ1-42 causes cell vulnerability and apoptosis.[19] However, in neurons, it has not been elucidated how extracellular Aβ raises cyto-

toxicity. One possible mechanism is that Aβ is internalized into neurons via endocytosis as observed in macrophages. Aβ1-42 is also reported to be internalized by endocytosis because of its high affinity to α7 nicotinic Ach receptor.[20] Another possible mechanism is the effect on ion channel currents, especially on Ca++ channels. There are many reports indicating that Aβ affects calcium homeostasis by blocking Ca++ influx at the plasma membrane or by perturbing Ca++ storage in the ER.[21–24] Therefore, it is possible that the UPR and proteasome dysfunction induced by extracellular Aβ is directly caused by the interaction of internalized Aβ in the cytosol. It is also possible that the UPR is induced by the disturbance of calcium homeostasis, a common cause of UPR.

Since proteasomal activity is deteriorated in postmortem brains of AD patients,[15] particular mechanisms may involve proteasomes in the pathology of AD. However, it is not clear whether proteasomal dysfunction is a cause or a result of AD. We here reported that Aβ disturbs proteasomal activity, and that the UPR by Aβ precedes proteasome dysfunction. We also suggested that the process may involve ERAD.

Oddo *et al.* reported that Aβ immunotherapy improves accumulations of Aβ, and at the same time improves tau pathology by clearing early hyperphosphorylated tau aggregates in the cytoplasm.[25] This effect is inhibited by a proteasome inhibitor, which indicates that Aβ is involved in tau pathology via proteasomes. Thus it is possible that Aβ deteriorates proteasomal activity, and leads cells to possibly accumulate phosphorylated tau and so be vulnerable to various insults. Our data suggest that proteasomal dysfunction by Aβ follows the UPR. Therefore certain therapeutic strategies for improving the UPR may have potential against AD pathology, as well as strategies for proteasomes.

It is not yet clear how extracellular Aβ causes the UPR. Further studies that shed light on this point should establish the hypothesis that amyloid pathology and tau pathology result via an ER-proteasome function.

REFERENCES

1 Haass C, De Strooper B. The presenilins in Alzheimer's disease – proteolysis holds the key (Review). *Science* 1999; **286**: 916–919.

2 Ebinu JO, Yankner BA. A RIP tide in neuronal signal transduction. *Neuron* 2002; **34**: 499–502.

3 De Strooper B. Aph-1, Pen-2, and Nicastrin with Presenilin generate an active gamma-Secretase complex (Review). *Neuron* 2003; **38**: 9–12.

4 Katayama T, Imaizumi K, Sato N *et al.* Presenilin-1 mutations downregulate the signalling pathway of the unfolded-protein response. *Nat Cell Biol* 1999; **1**: 479–485.

5 Imaizumi K, Miyoshi K, Katayama T *et al.* The unfolded protein response and Alzheimer's disease (Review). *Biochim Biophys Acta* 2001; **1536**: 85–96.

6 Paschen W. Endoplasmic reticulum: a primary target in various acute disorders and degenerative diseases of the brain (Review). *Cell Calcium* 2003; **34**: 365–383.

7 Nakagawa T, Zhu H, Morishima N *et al.* Caspase-12 mediates endoplasmic-reticulum-specific apoptosis and cytotoxicity by amyloid-beta. *Nature* 2000; **403**: 98–103.

8 Morishima N, Nakanishi K, Takenouchi H, Shibata T, Yasuhiko Y. An endoplasmic reticulum stress-specific caspase cascade in apoptosis. Cytochrome c-independent activation of caspase-9 by caspase-12. *J Biol Chem* 2002; **277**: 34287–33494.

9 Hitomi J, Katayama T, Eguchi Y *et al.* Involvement of caspase-4 in endoplasmic reticulum stress-induced apoptosis and Abeta-induced cell death. *J Cell Biol* 2004; **165**: 347–356. (Epub 2004 May 03.)

10 Friedlander R, Jarosch E, Urban J, Volkwein C, Sommer T. A regulatory link between ER-associated protein degradation and the unfolded-protein response. *Nat Cell Biol* 2000; **2**: 379–384.

11 Kostova Z, Wolf DH. For whom the bell tolls: protein quality control of the endoplasmic reticulum and the ubiquitin-proteasome connection (Review). *EMBO J* 2003; **22**: 2309–2317.

12 Nishikawa S, Brodsky JL, Nakatsukasa K. Roles of molecular chaperones in endoplasmic reticulum (ER) quality control and ER-associated degradation (ERAD) (Review). *J Biochem (Tokyo)* 2005; **137**: 551–555.

13 Jana NR, Nukina N. Recent advances in understanding the pathogenesis of polyglutamine diseases: involvement of molecular chaperones and ubiquitin-proteasome pathway (Review). *J Chem Neuroanat* 2003; **26**: 95–101.

14 Moore DJ, Dawson VL, Dawson TM. Role for the ubiquitin-proteasome system in Parkinson's disease and other neurodegenerative brain amyloidoses (Review). *Neuromolecular Med* 2003; **4**: 95–108.

15 Keller JN, Hanni KB, Markesbery WR. Impaired proteasome function in Alzheimer's disease. *J Neurochem* 2000; **75**: 436–439.

16 Bruce AJ, Malfroy B, Baudry M. β-Amyloid toxicity in organotypic cultures: protection by EUK-8, a synthetic catalytic free radical scavenger. *Proc Natl Acad Sci USA* 1996; **93**: 2312–2316.

17 Bence NF, Sampat RM, Kopito RR. Impairment of the ubiquitin-proteasome system by protein aggregation. *Science* 2001; **292**: 1552–1555.

18 Minagar A, Shapshak P, Fujimura R, Ownby R, Heyes M, Eisdorfer C. The role of macrophage/microglia and astrocytes in the pathogenesis of three neurologic disorders: HIV-associated dementia, Alzheimer disease, and multiple sclerosis (Review). *J Neurol Sci* 2002; **202**: 13–23.

19 Zhang Y, McLaughlin R, Goodyer C, LeBlanc A. Selective cytotoxicity of intracellular amyloid beta peptide1-42 through p53 and Bax in cultured primary human neurons. *J Cell Biol* 2002; **156**: 519–529.

20 Nagele RG, D'Andrea MR, Anderson WJ, Wang HY. Intracellular accumulation of beta-amyloid (1-42) in neurons is facilitated by

the alpha 7 nicotinic acetylcholine receptor in Alzheimer's disease. *Neuroscience* 2002; **110**: 199–211.
21 Arispe N, Pollard HB, Rojas E. beta-Amyloid Ca(2+)-channel hypothesis for neuronal death in Alzheimer disease (Review). *Mol Cell Biochem* 1994; **140**: 119–125.
22 Sun XD, Mo ZL, Taylor BM, Epps DE. A slowly formed transient conformer of Abeta (1-40) is toxic to inward channels of dissociated hippocampal and cortical neurons of rats. *Neurobiol Dis* 2003; **14**: 567–578.
23 Pierrot N, Ghisdal P, Caumont AS, Octave JN. Intraneuronal amyloid-beta1-42 production triggered by sustained increase of cytosolic calcium concentration induces neuronal death. *J Neurochem* 2004; **88**: 1140–1150.
24 Ferreiro E, Oliveira CR, Pereira C. Involvement of endoplasmic reticulum Ca2+ release through ryanodine and inositol 1,4,5-triphosphate receptors in the neurotoxic effects induced by the amyloid-beta peptide. *J Neurosci Res* 2004; **76**: 872–880.
25 Oddo S, Billings L, Kesslak JP, Cribbs DH, LaFerla FM. Abeta immunotherapy leads to clearance of early, but not late, hyperphosphorylated tau aggregates via the proteasome. *Neuron* 2004; **43**: 321–332.

WILEY InterScience
DISCOVER SOMETHING GREAT

Journal of Neuroscience Research 84:874–890 (2006)

Possible Role of Scavenger Receptor SRCL in the Clearance of Amyloid-β in Alzheimer's Disease

Kenji Nakamura,[1] Wakana Ohya,[1] Hiroshi Funakoshi,[1] Gaku Sakaguchi,[3] Akira Kato,[3] Masatoshi Takeda,[2] Takashi Kudo,[2] and Toshikazu Nakamura[1]*

[1]Division of Molecular Regenerative Medicine, Department of Biochemistry and Molecular Biology, Osaka University Graduate School of Medicine, Osaka, Japan
[2]Psychiatry, Department of Integrated Medicine, Division of Internal Medicine, Osaka University Graduate School of Medicine, Osaka, Japan
[3]Pain and Neurology, Discovery Research Laboratories, Shionogi and Co., Ltd., Shiga, Japan

Accumulation of β-amyloid protein (Aβ) in the brain is a hallmark of Alzheimer's disease (AD), and Aβ-mediated pathogenesis could result from increased production of Aβ or insufficient Aβ clearance by microglia, astrocytes, or the vascular system. Cell-surface receptors, such as scavenger receptors, might play a critical role in the binding and clearing of Aβ; however, the responsible receptors have yet to be identified. We show that scavenger receptor with C-type lectin (SRCL), a member of the scavenger receptor family containing coiled-coil, collagen-like, and C-type lectin/carbohydrate recognition domains, is expressed in cultured astrocytes and microglia. In contrast to the low expression of SRCL in the wild-type mouse brain, in a double transgenic mouse model of AD (Tg-APP/PS1), immunohistochemistry showed that SRCL was markedly induced in Aβ-positive astrocytes and Aβ-positive vascular/perivascular cells, which are associated closely with cerebral amyloid angiopathy. In patients with AD, the distribution of SRCL was similar to that seen in the Tg-APP/PS1 temporal cortex. The presence of a large number of SRCL/Aβ double-positive particles in the intracellular compartments of reactive astrocytes and vascular/perivascular cells in Tg-APP/PS1 mice and AD patients suggests a role for SRCL in Aβ clearance. Moreover, CHO-K1 cells transfected with SRCL isoforms were found to bind fibrillar $A\beta_{1-42}$. These findings suggest that SRCL could be the receptor involved in the binding or clearing of Aβ by glial and vascular/perivascular cells in AD.

Key words: scavenger receptor; SRCL; amyloid-β; astrocytes; microglia

Alzheimer's disease (AD) is a progressive neurodegenerative disorder (Tanzi and Bertram, 2005) characterized by accumulation of β-amyloid protein (Aβ) in the brain, which accumulation is thought to play a key role in the pathogenesis of AD. Aβ-associated pathogenesis may arise from the increased production of Aβ, or insufficient Aβ clearance by microglia, astrocytes, or the vascular system (Nicoll and Weller, 2003; Tanzi et al., 2004; Zlokovic, 2004; Tanzi and Bertram, 2005). Microglia and astrocytes have the ability to clear Aβ (Paresce et al., 1996; Guenette, 2003a,b; Wyss-Coray et al., 2003). For example, cultured wild-type mouse astrocytes were shown to bind to and contribute to the clearance of Aβ in Aβ-laden fresh brain sections of a transgenic mouse model of AD (Wyss-Coray et al., 2003); and a variety of substances can modulate Aβ clearance by microglia, astrocytes, and the vasculature, including antibodies against Aβ-peptide, TGFβ1, heat-shock proteins, apolipoprotein E (apoE), a monoclonal antibody against Aβ, and GM1 (Bard et al., 2000; Wyss-Coray et al., 2001; DeMattos et al., 2002; Kakimura et al., 2002; Matsuoka et al., 2003; Koistinaho et al., 2004). Antibodies against Aβ-peptide triggered microglial cells to clear plaques through Fc receptor-mediated phagocytosis and subsequent peptide degradation (Bard et al., 2000). These data show that Aβ can be eliminated from the brain, directly by glial cells, directly into the blood by vascular cells, or indirectly along perivascular interstitial fluid drainage channels and that the efficiency of Aβ clearance can be regulated. It has been postulated that increasing Aβ clearance may be a promising thera-

Supplementary Material for this article is available online at http://www.mrw.interscience.wiley.com/suppmat/0360-4012/suppmat/(www.interscience.wiley.com).

Contract grant sponsor: COE; Contract grant sponsor: Ministry of Education, Science, Technology, Sports and Culture of Japan and Ministry of Health and Welfare of Japan.

*Correspondence to: Dr. Toshikazu Nakamura, Division of Molecular Regenerative Medicine, Department of Biochemistry and Molecular Biology, Osaka University Graduate School of Medicine, B-7, Osaka 565-0871, Japan. E-mail: nakamura@onbich.med.osaka-u.ac.jp

Received 22 November 2005; Revised 10 May 2006; Accepted 23 May 2006

Published online 25 July 2006 in Wiley InterScience (www.interscience.wiley.com). DOI: 10.1002/jnr.20992

peutic approach to reduce Aβ-mediated pathogenesis in AD. Cell-surface receptors, such as scavenger receptors and related molecules, may play a critical role in the binding and clearance of Aβ; however, the putative receptors responsible for Aβ clearance have not yet been clearly identified (Paresce et al., 1996; Shibata et al., 2000; El Khoury et al., 2003; Alarcon et al., 2005).

Scavenger receptor with C-type lectin (SRCL) (Nakamura et al., 2001a, 2001b) is a member of the scavenger receptor (SR) family (Murphy et al., 2005), which members contain coiled-coil, collagen-like, and C-type lectin/carbohydrate recognition (CRD) domains. The predominant form of SRCL in humans was named human SRCL Type I (hSRCL-I). In contrast, the SRCL containing coiled-coil and collagen-like domains but lacking the CRD domain was termed human SRCL Type II (hSRCL-II) (Nakamura et al., 2001a). Because of structural similarities, SRCL is considered to be closely related to the Class A scavenger receptor (SR-A), which contains coiled-coil, collagen-like, and cysteine-rich domains (Kodama et al., 1990). The ability of SRCLs to bind Gram-negative and Gram-positive bacteria, as well as yeast, strongly suggests a role for SRCL in host defense (Nakamura et al., 2001a,b).

In the present study, we examined the possible participation of SRCL in the binding and clearance of Aβ in the AD brain. We provide the first evidence that SRCL is expressed, in an Aβ-dependent fashion, in astrocytes, microglia, and vascular/perivascular cells both in a double transgenic mouse model of AD (Tg-APP/PS1) and in cadaveric samples from patients with AD. We further show that SRCL could bind fibrillar $A\beta_{1-42}$ and that its expression was upregulated in the brains of patients with AD. We propose that SRCL may play an important role in Aβ binding, and presumably in clearance, by glial and vascular/perivascular cells in the AD-affected brain, acting in an Aβ dose-dependent manner.

MATERIALS AND METHODS

Animals

Timed pregnant Sprague-Dawley rats and C57/BL6 mice were purchased from SLC (Shizuoka, Japan). Double transgenic mice (Tg-APP/PS1) (Sakaguchi and Kudo, unpublished) and wild-type littermates (WT) were generated by crossing PS1 'knock-in' mice (Nakano et al., 1999) with transgenic mice (Tg2576) that overexpress the Swedish mutation of the human amyloid precursor protein (Hsiao et al., 1996). Animals were housed in individual cages in a temperature-controlled room under a 12-hr light/12-hr dark cycle. Procedures were approved by the Osaka University Graduate School of Medicine Ethics Committee. All efforts were made to minimize animal discomfort and the number of animals used.

Human Materials

Temporal cortex tissues from four cadavers with AD (average age at death = 84.2 ± 2.8) and three non-AD cortex samples (average age at death = 56.7 ± 26.1) were studied. All samples were obtained from the Brain and Tissue Bank of the University of Maryland and handled under procedures approved by the Institutional Review Board for Human Subject Research.

cDNA Cloning of Rat *SRCL* Coiled-Coil Region

Rat *SRCL* coiled-coil region sequence was cloned by PCR from hexaoligonucleotide primed cDNA of rat microglial total RNA by using the following primers: forward (F), 5′-GCAAGCAAATGGGGACTC-3′, corresponding to the putative coiled-coil initiation site of mouse *SRCL ORF* (residue 417), and reverse (R), 5′-AGGTGATGGGCTGTG-TAG-3′ corresponding to the putative coiled-coil ending site of *mSRCL* (residue 1070). PCR products were subcloned into pGEM-T vector (Promega, Madison, WI), and authenticity of the expression vector was confirmed by sequence analysis.

Northern Blot, RT-PCR, and Quantitative Real-Time RT-PCR Analyses

Total RNA was prepared from cells and tissues of adult and postnatal day 7 (P7) rats, as well as from temporal cortex of human autopsy samples, by using an ISOGEN Kit (Nippongene, Japan) or RNeasy Micro Kit (QIAGEN) according to the manufacturer's instructions. For Northern blotting, polyA+ RNA was prepared from total RNA of adult tissues; and 2 μg of polyA+ RNA was electrophoresed in a 1% agarose/0.7% formamide gel, blotted onto a Hybond N+ nylon membrane, and hybridized with ^{32}P-labeled cDNA fragment (nucleotides 493–1146 of human *SRCL*). Subsequently, the filter membrane was washed with high stringency, and visualized as previously described (Nakamura et al., 2001a,b). A rat *GAPDH* probe was used as a loading control.

For reverse transcription-PCR (RT-PCR), total RNA was pretreated with RNase-free DNase (Qiagen) and 1 μg selected RNA was reverse transcribed with SuperScript II (Invitrogen) and primed with random hexamers according to manufacturer's instructions. For rat experiments, after a 5-min denaturation at 95°C, 32 cycles of PCR amplification consisting of 94°C for 1 min, 58°C for 1 min, and 72°C for 1 min, followed by an extension phase of 72°C for 7 min, were carried out by using a GeneAmp Gold PCR Reagent Kit (Perkin-Elmer). The number of amplifications cycles and amount of cDNA used for each reaction were optimized for quantification of RNAs in preliminary experiments. PCR products were resolved by 1.5% agarose gel electrophoresis, and the gel was then stained with ethidium bromide. Rat *SRCL* primers were as follow: rat *SRCL*-forward (F), 5′-TTCTTTCCTCATCACCAC-3′; and rat *SRCL*-reverse (R), 5′-TGTTCACAATATCTGTCTC-3′. For normalization, *GAPDH* mRNA was used. For mouse experiments, the following RT-PCR protocol was used. After a 5-min denaturing incubation at 94°C, 32 cycles of PCR amplification consisting of 94°C for 30 sec, 63°C for 30 sec, and 72°C for 3 min, followed by an extension at 72°C for 5 min, was carried out by using the above reagent kit. Primers for mouse *SRCL* and mouse *GAPDH* were: mouse *SRCL-F*, 5′-ACACTGGTACGACTTCTCCGG-3′; mouse *SRCL-R*, 5′-CATTCTTCGGCTTTCAGAGGC-3′; mouse *GAPDH-F*,

5′-CGTGTTCCTACCCCCAATGT-3′; mouse *GAPDH-R*, 5′- TGTCATCATACTTGGCAGGTTTCT-3′. For real-time quantitative RT-PCR, 2.5 μg of each RNA was reverse transcribed by using SuperScript II (Invitrogen) according to manufacturer's instructions. For human autopsy samples, a High-capacity cDNA Archive Kit (Applied Biosystems, Foster City, CA) was used. Real-time RT-PCR was carried out with an ABI PRISM 7900 sequence detection system (Applied Biosystems) to quantify relative levels of mRNA in samples. For amplification of *hSRCL* and *GAPDH*, as an endogenous control, Universal PCR master mix (Applied Biosystems) and TaqMan MGB probes (FAM dye-labeled) were used for *hSRCL* (exon 5–6, Hs00560477m1; Applied Biosystems) and for human *GAPDH* (TaqMan VIC Probe; 4326317E; Applied Biosystems). All standards and samples were assayed in triplicate. Thermal cycling was initiated with an initial denaturation at 50°C for 2 min and 95°C for 10 min, followed by 40 cycles of PCR (95°C for 15 sec; 60°C for 1 min). Results were expressed as means ± standard error (SE) of the number of observations. Statistical significance was assessed by Student's *t*-test. A level of $P < 0.05$ was considered significant. Significance was determined after two separate experiments.

Cell Line Cultures

Cell lines CHO-K1, C6, J774A.1, and PC12 were cultured as described previously (Funakoshi et al., 1991; Naveilhan et al., 1996; Nakamura et al., 2001a,b).

Microglial Cultures

We prepared primary mixed-glia culture from newborn mice/rats (P1-3), and isolated primary astrocytes and microglia as described previously (Funakoshi et al., 2002). Mouse microglial cells were maintained in Dulbecco's modified Eagle's medium (DMEM) with 10% FBS. Rat microglial cells were maintained in serum-free modified N3, composed of high-glucose DMEM/Ham's F12 (DF) medium containing transferrin, insulin, progesterone, and sodium selenite (Funakoshi et al., 2002). In each primary microglial culture, microglial purity was approximately 95% as judged from Mac-1 (CD11b) immunostaining.

Preparation of Mouse Secondary Astrocytes

Primary astrocytes were prepared from P1 C57/BL6 mice largely as described previously (Funakoshi et al., 2002). Briefly, cerebral cortices were dissected, and the meninges were removed completely. The tissues were then minced, suspended in phosphate-buffered saline (PBS) containing 0.05% trypsin (GIBCO, Grand Island, NY) at 37°C for 10 min, and thereafter incubated with 0.01% DNase I (Sigma, St. Louis, MO) for 5 min at room temperature (RT). After incubation and centrifugation, the cell pellets were washed three times. Cells were filtered through a 75-μm nylon mesh, sedimented by centrifugation, suspended in low glucose DMEM (Nacalai tesque, Kyoto, Japan) containing 10% FBS (JRH Bioscience, Lenexa, KS), 100 IU/ml penicillin and 100 mg/ml streptomycin, and transferred to culture dishes. Once the cells had become confluent, they were rinsed with PBS, suspended in trypsin-containing PBS, and subcultured in DMEM/1% FBS in 6-well plates. After 3 days, the culture plates were rocked vigorously for 2 hr at RT to remove microglia. Astrocyte purity was >95% after 3 days in culture as judged from double immunostaining with anti-GFAP (Chemicon International, Temecula, CA) and anti-ionized calcium-binding adapter molecule-1 (IbaI) antibody (Wako Pure Chemical, Osaka, Japan).

fAβ Binding and Competition Assays

Human $fA\beta_{1-42}$ peptide (Seikagaku Kougyou, Tokyo, Japan) was dissolved in DMSO and diluted in sterile water to 1 mg/ml according to the manufacturer's instructions, and fibrillated just before usage. Twenty-four hours after isolation from primary mixed glial cultures, mouse microglial cells were treated at 37°C for 1 hr with 2.5 μg/ml $fA\beta_{1-42}$ in DMEM supplemented with 10% FBS. The cells were washed extensively with ice-cold PBS, fixed with 4% paraformaldehyde (PFA) in PBS, incubated with primary antibodies anti-CD11b (Mac-1) and anti-Aβ (6E10), followed by Alexa546 (red)- and Alexa488 (green)-conjugated secondary antibodies, counterstained with Hoechst 33342 (Molecular Probes), and observed under a LSM510 confocal microscope. Twenty-four hours after transfection with h*SRCL-I*, *-II*, m*SR-AI-Myc* or *Mock*-expression vector, CHO-K1 cells were treated at 37°C for 30 min with 2.5 mg/ml $fA\beta_{1-42}$ with or without 500 μg/ml Fucoidan, 200 μg/ml poly(C), or 200 μg/ml poly(G) in Ham's F12 medium supplemented with 10% FBS. The cells were visualized with anti-Myc (12A5) and anti- fAβ antibody as described above.

fAβ Treatment of Primary Mouse Astrocytes

Human $fA\beta_{1-42}$ peptide was dissolved in DMSO and diluted in PBS to 300 mM, corresponding to 1.35 mg/ml, and incubated for 3 days at 37°C, and subsequently sonicated when required, to prepare fAβ.

Preparation of Antibody

The synthetic peptide QPD (KAGQPDNWGHGHGP-GEDC) (Nakamura et al., 2001a), corresponding to a part of the CRD region of the hSRCL, was obtained from MBL (Osaka, Japan) (Fig. 4A). Rabbits were immunized with the QPD peptide coupled to keyhole limpet hemocyanin (KLH) by M-maleimidobenzol-*N*-hydroxysuccinimide ester. The antiserum was purified on an affinity column of CNBr-activated Sepharose4B (Amersham) coupled to the immunogen without KLH and referred to here as anti-SRCL antibody (OT667).

Western Blot Analysis

Twenty-four hours after transfection with the desired constructs, CHO-K1 cells and J774A.1 cells were lysed. The lysates were electrophoresed under reducing conditions, and then immunoblotted with anti-SRCL antibody. An ECL system was used for visualization.

Immunohistochemistry

Mice were deeply anesthetized and transcardially perfused with cold PBS followed by cold 4% PFA in PBS. The brains were removed and postfixed for 1.5 hr at 4°C and separated at the midline into halves. One half was immersed in a series of sucrose (10%, 20%) in PBS and frozen in CO_2 gas to prepare frozen sections. The other half was dehydrated and embedded in paraffin according to standard procedures and cut into sections. For human materials, 10% formalin-fixed brain tissues were embedded in paraffin and cut into sections. Paraffin sections were deparaffinized and rehydrated by sequential 5-min incubation in 100%, 95%, and 75% ethanol. The sections were then rinsed twice in water and twice in PBS. Endogenous peroxidase activity was quenched by incubation for 5 min with 3% H_2O_2. To unmask antigens, we immersed the slides for 10 min at RT in 50 mM Tris-HCl (pH 8.0) containing 0.4 mg/ml Proteinase K and then washed them in PBS. Sections were blocked for 30 min at RT with blocking buffer consisting of 5% normal goat serum and 0.3% Triton X-100 in PBS. For Aβ immunostaining, sections were pre-treated with 70% formic acid for 1 min, blocked with blocking buffer and incubated with primary antibodies for 1.5 hr at RT. The following antibodies were used: affinity-purified rabbit anti-SRCL (OT667, 3 mg/ml), mouse anti-GFAP (1:400; MAB3402; Chemicon, for astrocytes), rat anti-Mac-1 (1:100; Chemicon;, for microglia and macrophage including MATO cells), rabbit anti-Iba-1 (1:1,000; WAKO, Japan;, for microglia and macrophages including MATO cells), mouse anti-rat CD-31 (1:200; PECAM-1; Pharmingen; activated, Lewis rat-derived microglia as immunogen, for activated microglia/macrophages, MATO and endothelial cells), anti-αSMA (1:500; DAKO; for smooth muscle cells), and rabbit anti-Aβ40 (1:1,500; FCA3340) and rabbit anti-Aβ42 (1:1,500; FCA3542) antibodies (FCA3340 and FCA3542 were kindly provided by Dr. F. Checler). After having been washed three times with PBS, the sections were incubated for 20 min at RT with secondary antibodies conjugated with Alexa488 (green) or Alexa546 (red), and subsequently washed with PBS and mounted.

Human tissue sections were visualized as brown signals by incubation with the EnVision+ System (K4001 for mouse/K4003 for rabbit; Dako, Glostrup, Denmark) and 3,3′-diaminobenzidine tetrahydrochloride (DAB; Wako, Japan) as the chromogen. For double labeling immunohistochemistry, after visualization of the first primary antibody with DAB, sections were microwaved for 5 min in citrate buffer (pH 6.0), and then were washed and incubated with the second primary antibody. Samples were visualized as pink signals by using an alkaline phosphatase-conjugated anti-rabbit IgG (Vector, CA) and a Vector Red Alkaline Phosphatase Substrate Kit according to the manufacturer's instructions, and counterstained with Mayer's hematoxylin (WAKO). For preabsorption, some sections were incubated with anti-SRCL antibody that had been pre-absorbed with an excess amount of immunogen. For double immunostaining of $A\beta_{1-40}/A\beta_{1-42}$ and SRCL, rabbit anti-$A\beta_{1-40}/A\beta_{1-42}$ antibodies and affinity-purified rabbit anti-SRCL antibody were labeled with Alexa546 and Alexa488, respectively, by using a Zenon Alexa Fluor Rabbit IgG Labeling Kit (Molecular Probes) according to the manufacturer's instructions and used for direct immunofluorescence staining.

RESULTS

cDNA Cloning of Rat *SRCL* Coiled-Coil Region

We first wished to compare the sequence of the region of rat *SRCL* cDNA encoding the coiled-coil domain with human and mouse sequences. We carried out RT-PCR using cDNA generated from rat microglial cells amplified with primers based on mouse *SRCL* cDNA. The cloned cDNA corresponding to the rat *SRCL* coiled-coil domain was highly similar to that of human and mouse *SRCLs*, with 88% and 95% identity, respectively, at the nucleotides level, 91.7% and 95.9% identity, respectively, at the amino acid level, and containing 8 putative *N*-glycosylation sites. This degree of conservation suggests that the glycosylation sites are important for folding, maturation, or function of the SRCL protein.

Rat *SRCL* mRNA Is Expressed in Various Tissues as a Single Transcript

Human *SRCL* is transcribed as 2 different isoforms, i.e., human *SRCL* type I (h*SRCL-I*) and *SRCL* type II (h*SRCL-II*). *hSRCL-I*, containing a C-type CRD, is the major transcript found in human tissues; and it is resolved as a 3.0-kb species by Northern blotting. In contrast, h*SRCL-II*, which lacks the C-type CRD, exhibits a 4.5-kb species on Northern blots. Mouse *SRCL* is resolved as a single 3.0-kb transcript corresponding to h*SRCL-I*; and no other transcripts are seen, suggesting that mice express only one isoform. We examined various rat tissues for expression of *SRCL* isoforms using Northern blotting. *SRCL* mRNA was widely expressed in them. Using a probe targeting the coiled-coil region of rat *SRCL*, we found its mRNA to be resolved as a single 3.0-kb band (Fig. 1). Expression was highest in the lung, followed by the spleen, small and large intestine, stomach, and brain; whereas rat *SRCL* mRNA expression was below detection limits in the liver. Thus, like mice, rats expressed only one *SRCL* transcript, which corresponded to h*SRCL-I*.

Rodent Microglia and Astrocytes Express *SRCL* mRNA

It has been suggested that microglia and astrocytes in the brains of patients with AD are associated with senile plaques and contribute to recognition, ingestion, and elimination of fibrillar β-amyloid peptide (fAβ) from plaques. This could be facilitated by scavenger receptors on the cell surface. To determine whether these cells express SRCL, we examined *SRCL* mRNA expression in cultured rodent microglia (Fig. 2A,B) and astrocytes by using semiquantitative RT-PCR. After a 24-hr culture period (1 day in vitro, 1DIV), *SRCL* mRNA was detected in astrocytes (ASTRO) and at 2DIV in microglia (MG, 2-day culture; Fig. 2C). In contrast, *SRCL* mRNA expression was below the detection limit in neurons (PC12 cells) and C6 glioma cells (Fig. 2C). These findings show that *SRCL* mRNA was primarily expressed in glial cells but not in neurons among neural

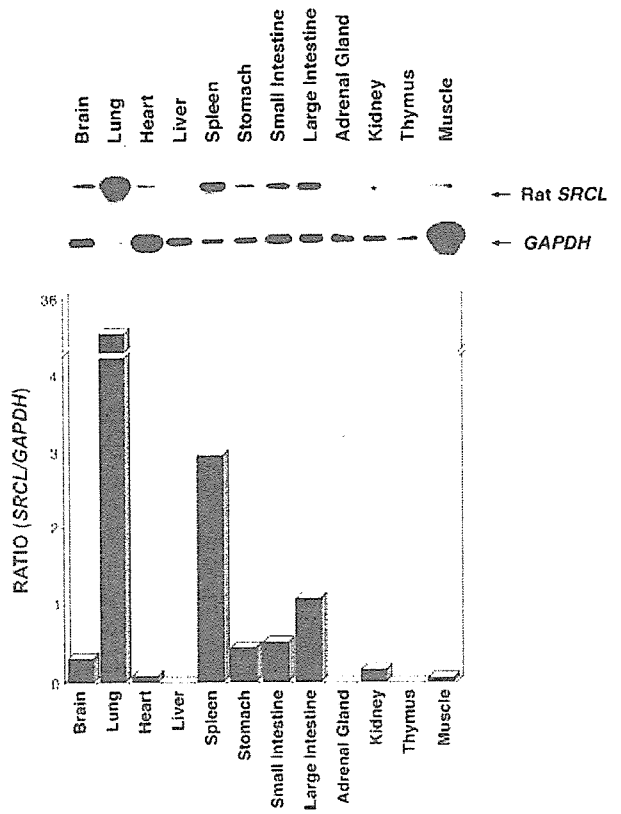

Fig. 1. Northern blot analysis of rat *SRCL* mRNA in various adult rat tissues. **Upper panel:** rat *SRCL* is widely expressed as a single 3.0-kb transcript. Highest expression of mRNA was detected in lung followed by spleen, intestine, stomach, and brain. *GAPDH* served as a loading control. **Lower panel:** level of *SRCL* mRNA relative to *GAPDH* mRNA is presented based on the densitometry analysis.

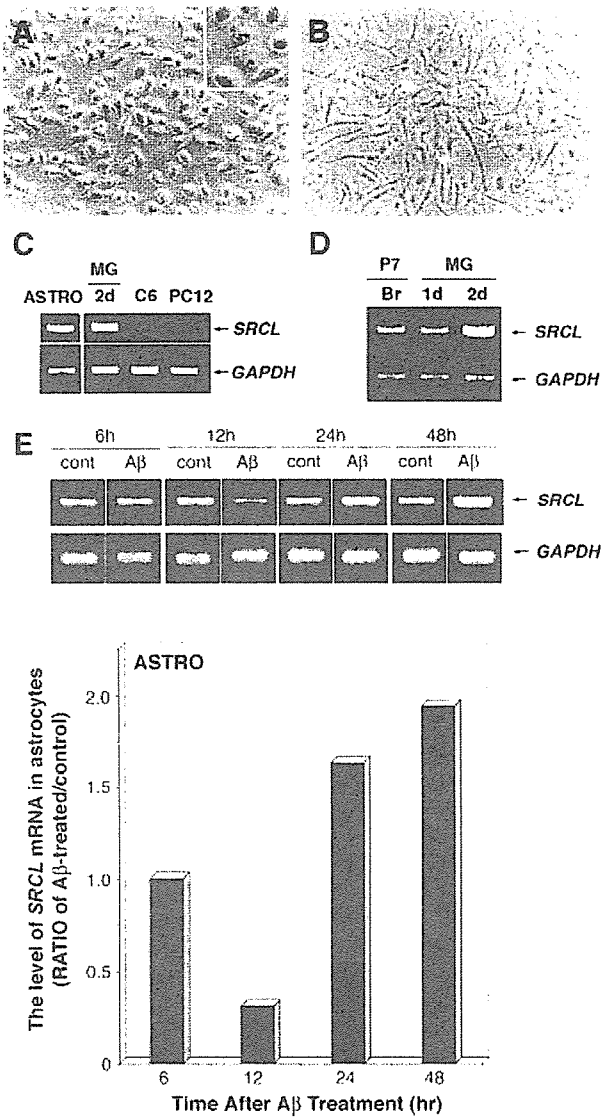

Fig. 2. RT-PCR analysis of *SRCL* mRNA in cultured neonatal microglia and astrocytes. **A,B:** Representative photomicrographs of rat neonatal microglia (MG) after 15 min (A inset, high-magnification view) and 2 days in primary culture (B). **C:** RT-PCR of cultured neural cells: mouse neonatal astrocytes (ASTRO), rat neonatal microglia (MG), human C6 glioma (C6) and rat pheochromocytoma PC12. RT-PCR showed that *SRCL* mRNA expression is prominent in ASTRO and MG, but under the detection limits in C6 and PC12. **D:** RT-PCR of rat *SRCL* mRNA in cultured neonatal microglia at different times after the start of the culture. The level of *SRCL* mRNA was increased at 2 days after the start of the culture (2d) compared to that at 1 day (1d) and the former level became higher than postnatal day 7 (P7) brain (Br). **E:** RT-PCR of cultured astrocytes treated with $fA\beta_{1-42}$. The level of *SRCL* mRNA in astrocytes was increased at 48 hr after $fA\beta_{1-42}$ application. *GAPDH* served as a loading control. The ratio of rat *SRCL* mRNA levels (Aβ-induced level vs. matched control level) is expressed in the lower panel.

cells in vitro. In addition, we found that the level of *SRCL* mRNA increased in a culture time-dependent manner (MG) or was regulated by the application of amyloid-β peptide (ASTRO). In microglia, *SRCL* mRNA expression levels increased during the culture time, and the level at 2 days of culture was higher than that in the brain (Br) at postnatal day 7 (P7; Fig. 2D); i.e., the level increased at 2 days of culture when the cultured microglia showed activated morphology as compared to that at 1 day (Fig. 2B,A, respectively). It seems likely that the level of *SRCL* mRNA in microglia is correlated with the state of microglial activation. To determine whether $fA\beta_{1-42}$ could alter the expression of *SRCL* mRNA, we treated cultured mouse neonatal astrocytes with $fA\beta_{1-42}$ for the times indicated in Figure 2E, and analyzed expression of *SRCL* mRNA. Using semiquantitative RT-PCR, we observed that the *SRCL* mRNA level increased at 48 hr after $fA\beta_{1-42}$ treatment relative to that of the matched control astrocytes (Fig. 2E). Similar results were obtained when the other primer set for *SRCL* mRNA was used (data not shown).

The induction levels of *SRCL* mRNA in microglia were almost comparable to that of astrocytes in vitro (1.9 vs. 2.4). Taken together with our previous finding that SRCL acts as a scavenger receptor (Nakamura et al., 2001a,b), these results suggest that SRCL-expressing activated glial-cells may recognize a variety of substances in neurodegenerative tissues, such as fAβ in the AD-affected brain.

Mouse Primary Microglia Bind and Ingest Synthetic $fA\beta_{1-42}$ Microaggregates

To determine the role of SRCL expressed in activated glial cells in the recognition of $fA\beta_{1-42}$, we developed positive-control conditions in which fibrillar $A\beta_{1-42}$ was recognized and ingested by primary microglia. When we incubated primary microglia for 1 hr with $fA\beta_{1-42}$ prepared from synthetic $A\beta_{1-42}$ peptides by a 3-day incubation at 37°C, we observed a high degree of cellular binding and ingestion of $fA\beta_{1-42}$ microaggregates (Supplementary Fig. 1).

Human SRCL-I and SRCL-II Expressed in CHO-K1 Cells Bind $fA\beta_{1-42}$

To investigate whether SRCL would have the ability to bind $fA\beta_{1-42}$, we examined $fA\beta_{1-42}$ binding by CHO-K1 cells transiently expressing hSRCL-I in the presence or absence of Fucoidan, one of the major ligands for scavenger receptors (SRs). CHO-K1 cells expressing mouse Class A Type I scavenger receptor (mSR-AI) served as a positive control for the assay. CHO-K1 cells transiently transfected with m*SR-AI-Myc* or h*SRCL-I-Myc* were incubated with $fA\beta_{1-42}$ for 1 hr at 37°C. After extensive washing with PBS, the cells were fixed and processed for immunostaining with antibodies against $fA\beta_{1-42}$ and Myc to visualize mSR-AI-Myc or hSRCL-I-Myc. The $fA\beta_{1-42}$ binding (green color) was specifically seen in CHO-K1 cells expressing mSR-AI-Myc or hSRCL-I-Myc (red color), whereas the binding was markedly competed in the presence of an excess amount of Fucoidan (Fig. 3A). To further confirm the ability of SRCL to bind $fA\beta_{1-42}$, we generated CHO-K1 cells stably expressing m*SRCL-Flag* (*Flag-tag* was fused to the cytosolic end of m*SRCL*). A similar result was obtained when Cy3-labeled-$fA\beta_{1-42}$ (Cy3-$fA\beta_{1-42}$) binding to CHO-K1 cells stably expressing mSRCL was examined (Supplementary Fig. 2). In contrast to the failure of the parental CHO-K1 cells to bind Cy3-$fA\beta_{1-42}$, CHO-K1 cells stably expressing mSRCL showed strong binding capacity for Cy3-$fA\beta_{1-42}$ (red color), and this binding was competed by Fucoidan (Supplementary Fig. 2). These findings show that SRCL specifically bound to $fA\beta_{1-42}$ by using the same residues interacting with other scavenger receptor ligands, such as Fucoidan.

To further investigate whether the CRD region of SRCL would be essential for the binding of $fA\beta_{1-42}$ to SRCL, we examined $fA\beta_{1-42}$ binding to CHO-K1 cells transfected with m*SR-AI-Myc*-, h*SRCL-I-Myc*, h*SRCL-II-Myc*-, or *Mock*-expression vectors. Interestingly, in addition to CHO-K1 cells expressing mSR-AI, those cells expressing either isoform of hSRCL efficiently bound $fA\beta_{1-42}$, but *Mock*-transfected cells did not (Fig. 3B). Given the differences in domain composition between hSRCL-I and -II, it seems that $A\beta_{1-42}$ binding was primarily mediated by SRCL collagenous domains and that the CRD of hSRCL-I contributed relatively little to the binding. Finally, we examined $fA\beta_{1-42}$ binding to these cells in the presence of polyguanylic acid (poly(G)), a ligand for scavenger receptors that inhibits $fA\beta_{1-42}$ binding to the polycationic region of the collagenous domain of SR-AI. Poly(C) served as a negative control. The binding of $fA\beta_{1-42}$ to CHO-K1 cells expressing mSR-AI was not inhibited by 200 μg/ml poly(C) but was inhibited by 200 μg/ml poly(G). To see whether hSRCL binding to $fA\beta_{1-42}$ was mechanistically similar to binding by mSR-AI, we carried out the same assay with cells expressing hSRCL-I or -II. In contrast to the results for mSR-AI, the binding of $fA\beta_{1-42}$ by cells expressing either isoform was not sensitive to poly(G) (200 μg/ml; Fig. 3B). Although we cannot exclude the possibility that hSRCL-I and -II bind to $fA\beta_{1-42}$ differently than does mSR-AI, we consider the most likely explanation for this difference to be the larger number of polycationic regions in the collagenous domain of SRCL (three domains) versus the single domain in SR-AI and thus it seems likely that the binding affinity of SRCLs to $fA\beta_{1-42}$ might be higher than that of SR-AI, as seen in the Poly(G) competition assay.

Immunohistochemical Localization of Mouse SRCL in Tg-APP/PS1

For immunolocalization of SRCL protein in AD-affected brains, we generated a rabbit anti-hSRCL polyclonal antiserum specific for the QPD sequence of the CRD region of hSRCL (Nakamura et al., 2001a,b). The antiserum was purified by using an affinity column bearing the immunized peptide and the resultant purified antibody is referred to hereafter as anti-SRCL antibody. Because hSRCL-I and mSRCL but not hSRCL-II have the CRD region containing the QPD sequence, this anti-SRCL antibody was expected to recognize specifically hSRCL-I and mSRCL (Fig. 4A).

Western blot analysis using the anti-SRCL antibody showed that this antibody recognized the SRCL protein in human *SRCL-I-Myc/EGFP*-transfected cells (h*SRCL-I-Myc/EGFP*), mouse *SRCL-Myc/EGFP*-transfected cells (m*SRCL-Myc/EGFP*), and J774A.1 mouse macrophage at the expected molecular size but not that in *Mock/EGFP*-transfected cells or h*SRCL-II-Myc/EGFP*-transfected cells (Fig. 4B). The small differences seen in the molecular weight of the reactive proteins may reflect differences in glycosylation patterns. To further confirm the specificity of this antibody, we immunostained *hSRCL-I-Myc/EGFP*-, h*SRCL-I-Myc/EGFP*- and *mSRCL-Myc/EGFP*-transfected CHO-K1 cells with anti-SRCL antibody. Immunostaining of the transfected

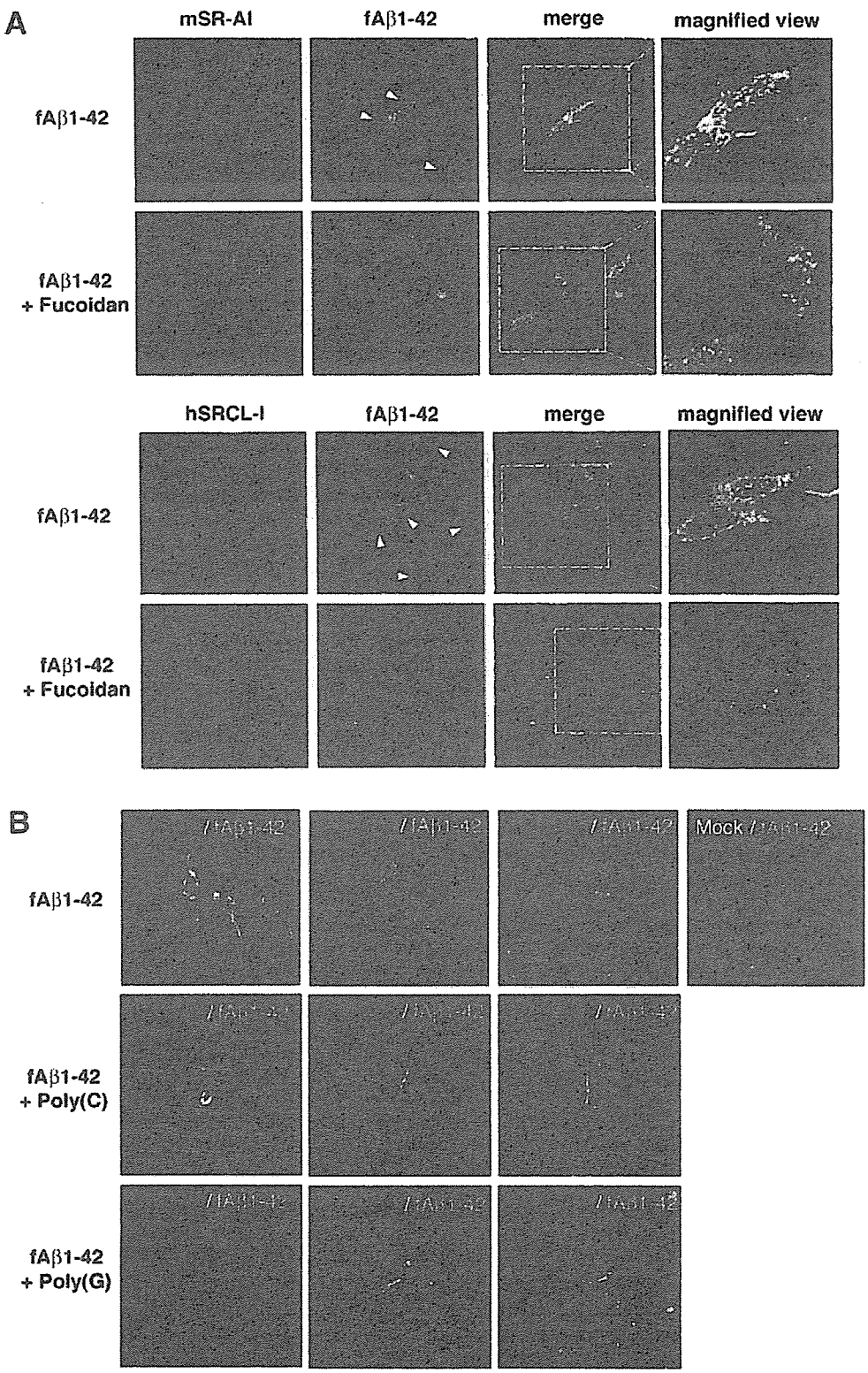
A
mSR-AI
fAβ1-42
merge
magnified view
fAβ1-42
fAβ1-42
+ Fucoidan
hSRCL-I
fAβ1-42
merge
magnified view
fAβ1-42
fAβ1-42
+ Fucoidan
B
fAβ1-42
Mock
fAβ1-42
fAβ1-42
+ Poly(C)
fAβ1-42
+ Poly(G)

Figure 3.

cells showed that this antibody recognized CHO-K1 cells transiently expressing hSRCL-I-Myc/EGFP or mSRCL-Myc/EGFP but did not recognize CHO-K1 cells expressing Mock/EGFP or hSRCL-II-Myc/EGFP (Fig. 4C). In addition, preabsorption of anti-SRCL antibody with immunogen eliminated the ability of this antibody to recognize CHO-K1 cells expressing hSRCL-I-Myc/EGFP (Fig. 4C). These observations clearly show the specificity of the anti-SRCL antibody for hSRCL-I and mSRCL.

Using this antibody, we examined the immunolocalization of SRCL in Tg-APP/PS1, a double transgenic mouse model of familial AD that coexpresses a mutated amyloid-beta precursor protein and a mutated form of human presenilin-1. In wild-type littermates, we observed no specific SRCL-immunoreactivity (IR) in microglia and astrocytes located in the cerebral cortex (Fig. 5A,B, upper panel, arrow), except for the specific staining for SRCL in perivascular macrophages (MATO cells; data not shown; Fig. 6C, arrowheads). In contrast, a large amount of SRCL-IR was visualized in GFAP-positive, plaques-surrounding reactive astrocytes in both cerebral cortex and hippocampus of 9-month-old Tg-APP/PS1 (Fig. 5A). The intensity of SRCL-IR was strong in GFAP-positive astrocytes situated close to Aβ plaques (Fig. 5A, arrowheads), but weak in those located far away from such Aβ plaques (Fig. 5A, arrows). These data are consistent with our finding that Aβ increased SRCL level in astrocytes in vitro (Fig. 2E). In contrast, SRCL-IR was not detected in wild-type mice and was only weakly present in neurons in amyloid CA1 regions of the hippocampus in association with Aβ-plaque in 9-month-old Tg-APP/PS1 (Fig. 5A, lowest panel). In microglia, SRCL-IR was under the detection limit in wild-type mice (Fig. 5B, upper panel); whereas slight upregulation of SRCL-IR in microglia was seen in association with Aβ plaques in Tg-APP/PS1 in vivo (Fig. 5B, lower panel, arrowhead). These findings suggest that SRCL would play an important role in glial cells such as astrocytes and microglia in AD.

Next we examined whether SRCL could be induced in cells after the development of cerebral amyloid angiopathy (CAA), a typical pathologic feature in AD, by double-immunostaining for SRCL and $A\beta_{1-42}$ or $A\beta_{1-40}$ in the cerebral cortex of 9-month-old Tg-APP/PS1 mice and their wild-type littermates. In age-matched wild-type littermates, no specific staining for Aβ-IR or SRCL-IR was seen inside the leptomeningeal vessel (m.v.; Fig. 6A, upper panel, arrowhead), except for the specific staining for SRCL in perivascular macrophages (MATO cells; data not shown). In contrast, colocalization of SRCL-IR and $A\beta_{1-42/1-40}$ was evident specifically in leptomeningeal vessels showing characteristics of CAA in Tg-APP/PS1 mice (Fig. 6A, arrows). At high magnification, SRCL-IR and $A\beta_{1-40}$-IR appeared as particles; many were colocalized inside the vessel wall, suggesting the possibility of internalization of Aβ by SRCL on vascular/perivascular cells (Fig. 6A, inset). Sections incubated without first antibody eliminated this staining, confirming the specificity of the SRCL-IR (Fig. 6A, lowest panel).

Figure 6B shows a schematic representation of the vascular/perivascular cells in leptomeningeal vessel (m.v.) of wild-type mice and Tg-APP/PS1. In wild-type mice, the m.v. contains endothelial cells (ECs: light green) that are surrounded by smooth muscle cells (SMCs: orange), and its vessel wall is thin. Beside the vessel, perivascular macrophage (MATO cell: yellow) is present. In the m.v. of Tg-APP/PS1, a large amount of Aβ (red) is localized within the vascular wall. Many macrophages (MØ: yellow) having attached to the outer surface of and infiltrated into the vascular wall, the number of SMCs has increased and the vessel wall becomes thicker during the progression of disease. It is of note that the vascular/perivascular cells contain multiple Aβ particles (red) inside the cells, possibly as a result of ingestion. These Aβ-containing cells include not only macrophage (MØ) and MATO cells, but also SMCs and ECs. Despite the knowledge of Aβ localization, the molecules responsible for Aβ binding and ingestion are not well defined.

Because SRCL-IR was colocalized with $fA\beta_{1-40/1-42}$-IR within Tg-APP/PS1-vessels (Fig. 6A), we next assessed which vascular/perivascular cells expressed SRCL by using vascular/perivascular cell-specific antibodies: anti-rat CD31 (activated Lewis rat microglia as immunogen, a marker for microglia/macrophage including MATO cells and ECs), anti-αSMA (for SMCs), and anti-GFAP antibody (for astrocytes). In wild-type littermates, we did not easily observe SRCL-IR (green) co-present with CD31-IR (red; Fig. 6C. upper panel), except for MATO cells (Fig. 6C, arrowheads). SRCL-IR was only weakly detected in αSMA-positive SMCs and fairly well detected in CD31-positive ECs in the m.v. of wild-type littermates (Fig. 6C, middle and upper panels, respectively). In contrast to wild-type littermates, we could detect strong SRCL-IR (green) in subpopula-

Fig. 3. Binding of synthetic fibrillar $A\beta_{1-42}$ to CHO-K1 cells expressing *hSRCL-I* or *-II* and competition by poly(G). **A:** hSRCL-I mediates $fA\beta_{1-42}$ binding to CHO-K1 cells, and the binding is eliminated by Fucoidan. m*SR-AI-Myc,*- or h*SRCL-I-Myc*-transfected-CHO-K1 cells treated with $fA\beta_{1-42}$ were visualized with anti-Myc and anti-Aβ antibodies followed by Alexa546 (red)- and Alexa488 (green)-conjugated antibodies, respectively. Synthetic $fA\beta_{1-42}$ microaggregates (green) specifically bound to m*SR-AI-Myc*- and h*SRCL-I-Myc*-expressing cells (red). Nuclei (in blue) were counterstained with Hoechist33342. **B:** Competition assays with poly(C) or poly(G). m*SR-AI-Myc*-, h*SRCL-I-Myc*-, h*SRCL-II-Myc*- or *Mock*-transfected CHO-K1 cells were incubated with PBS containing $fA\beta_{1-42}$ and an excess amount of poly(C) or poly(G), and the cells were then visualized with anti-Myc and anti-Aβ antibodies detected with Alexa546 (red)- and Alexa488 (green)-conjugated antibodies, respectively. Synthetic $fA\beta_{1-42}$ microaggregates (green) specifically bound to m*SR-AI-Myc*- h*SRCL-I-Myc*-, and h*SRCL-II-Myc*-expressing cells (red), but not to mock-transfected cells. Poly(G) (200 μg/ml) but not poly(C) (200 μg/ml) could efficiently compete the binding of $fA\beta_{1-42}$ to cells expressing m*SR-AI*, whereas neither poly(G) nor poly(C) could efficiently compete that to cells expressing h*SRCL-I* or h*SRCL-II*.

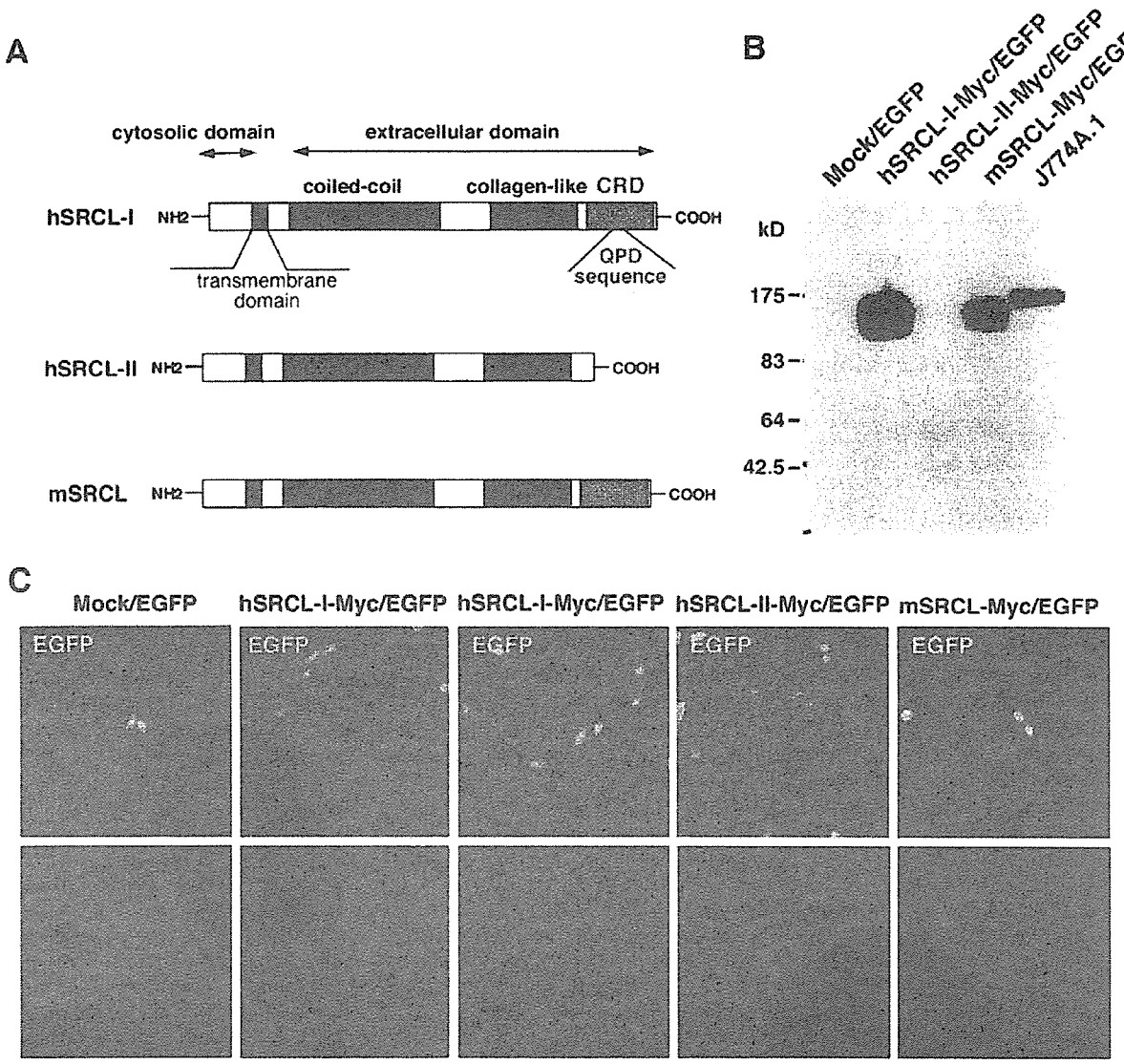

Fig. 4. Western blotting and immunocytochemistry with anti-hSRCL antibody. **A:** Schematic representation of the domain structure of hSRCL-I, hSRCL-II and mSRCL showing the position used as the immunogen for anti-SRCL antibody. CRD, carbohydrate recognition domain. Anti-SRCL serum was raised against the peptide containing the QPD sequence at the CRD of hSRCL, purified by using an affinity column of immunogen; and referred to as anti-SRCL antibody. **B:** Western blotting. CHO-K1 cells were transiently transfected with expression vectors for hSRCL-I-Myc/EGFP, hSRCL-II-Myc/EGFP, mSRCL-Myc/EGFP, and Mock/EGFP. Equal amounts of extracts from the cells were loaded for SDS-PAGE. Western blot analysis was carried out by using the anti-SRCL antibody. J774A.1 cells, a mouse macrophage cell line. **C:** Immunocytochemistry. CHO-K1 cells were transiently transfected with the indicated expression vectors. Two days after the transfection, the cells were fixed in 4% PFA in PBS and immunostained with anti-SRCL antibody and subsequently with Alexa546-conjugated secondary antibody (red), with or without preabsorption of the primary antibody with an excess amount of immunogen.

tions of vascular/perivascular cells of Tg-APP/PS1 mice (Fig. 6D,E). In Tg-APP/PS1, in addition to CD31-IR along with SRCL-IR in MATO cells, SRCL-IR became intense inside the meningeal vascular wall in which infiltrating macrophages had accumulated and in ECs (Fig. 6C, upper panel. arrows; red), suggesting induction of SRCL in macrophages. At high-magnification (Fig. 6D, upper panel), SRCL-IR (green) appeared as multiple particles inside CD31-positive macrophages (red) that had accumulated within the vessel wall, indicating internalization of SRCL by macrophages. SRCL-IR intensity (green) was markedly increased in αSMA-